INSTITUTE OF PHYSICS PUBLISHING SEMICONDUCTOR SCIENCE AND TECHNOLOGY
Semicond. Sci. Technol. **19** (2004) 494–500 PII: S0268-1242(04)65440-X

Comparison of surface and bulk contributions to non-radiative currents in InGaAs/AlGaAs laser diodes

G Beister and H Wenzel

Ferdinand-Braun-Institut für Höchstfrequenztechnik, Albert-Einstein-Str. 11, 12489 Berlin, Germany

Received 27 June 2003
Published 2 February 2004
Online at stacks.iop.org/SST/19/494 (DOI: 10.1088/0268-1242/19/3/037)

Abstract
We present novel investigations of surface and bulk contributions to the non-radiative recombination in InGaAs/AlGaAs ($\lambda = 0.98\ \mu$m) RW laser diodes. These enable us to explain earlier experiments, in which we extracted the non-radiative and the radiative current components from the power–voltage–current (*P*–*V*–*I*) characteristics measured well below the threshold. From these experiments, the non-radiative current component was identified as primarily related to surface recombination, which increased during facet degradation, and could be decreased by a sulfur treatment. In this paper, we use these experimental results to estimate the drop of the surface recombination velocity after the sulfur treatment and to give an upper bound for the bulk carrier lifetimes. This is done by simulations of the *V*–*I* characteristics assuming that all non-radiative recombination takes place either at the surface or in the bulk.

1. Introduction

Nowadays, due to the high quality of epitaxial layers produced by modern growth and processing technologies, the lifetime of semiconductor lasers is limited by the formation of internal crystal defects in the bulk or at the facets of the laser structures. Non-radiative recombination via point defects, and enhanced defect reactions induced by these recombination events [1–4], are the general origin of possible degradation processes during laser ageing. The well-known catastrophic optical mirror damage (COMD) is related to such non-radiative recombination via surface defects, which leads in combination with an additional optical self-absorption to a growing number of recombination centres and finally to a thermal runaway at the facets [5–7]. Therefore, technological efforts towards an increase of the facet stability have to be focused on the minimization of surface recombination, for example by facet passivation measures [8] or by an introduction of window regions adjacent to the facets with reduced current injection and absorption [9]. In order to evaluate the success with such efforts, techniques are needed that provide information on the facet stability.

Some years ago, we presented a non-destructive method which enabled the separate determination of radiative, I_r, and non-radiative, I_{nr}, current components in laser diodes and which delivered information on the electronic facet stability via monitoring I_{nr} [10]. To extract both current components, we used measurements of the emission power, *P*, in dependence on the voltage, *V*, well below the threshold and an iterative analysis based on earlier theoretical models [11] and [14] which will be described shortly in section 2. With this method, we were able to demonstrate that changes of I_{nr} in the low-current region corresponded very sensitively to changes of the electronic facet stability and that facet degradation during ageing became observable by measurements of I_{nr} well before COMD occurred. The experiments were carried out at InGaAs/AlGaAs ridge waveguide (RW) laser structures. We realized, by surface treatments with NH_4S_x resulting in a decrease of I_{nr} over more than one order of magnitude, that the observed changes, ΔI_{nr}, of I_{nr} are due to surface reactions only [11, 12].

However, for laser diode structures there is no exact information on the quantitative change of surface recombination due to facet degradation or special surface treatments at present. To our knowledge, measurements of surface recombination velocities are usually performed on broad area wafer samples or special structures, as described in [13] for GaAs/AlGaAs heterojunction bipolar

© 2004 IOP Publishing Ltd Printed in the UK

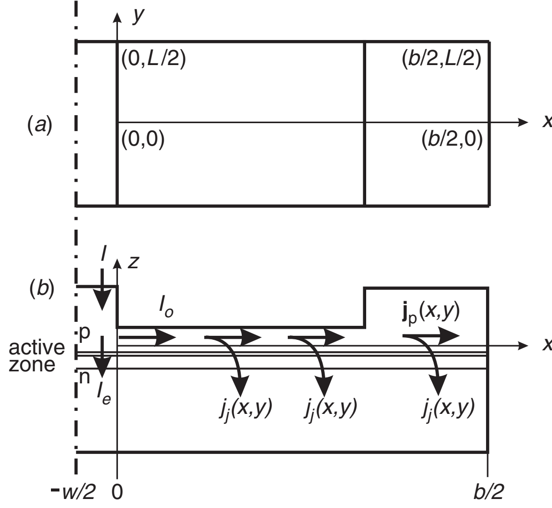

Figure 1. Schematic top (*a*) and front (*b*) view of the ridge waveguide laser structure under investigation. The coordinate system underlying the simulations and the different components of the electrical current and current density are shown.

transisitors, which were sensitively affected by changes of surface conditions. In our experiments where the (110) and (−110) surfaces of laser diodes were treated with NH_4S_x the question was open whether the remaining I_{nr} results from surface recombination (albeit reduced) or is already limited by non-radiative recombination in the bulk.

To answer this question, simulations of the subthreshold voltage–current characteristics of the laser diodes are necessary, taking into account surface as well as bulk non-radiative recombination. But a general three-dimensional (3D) model of laser diodes, which would allow us to treat surface and bulk effects on an equal footing, is not available. Therefore, we have used two models—one for the surface and the other for the bulk contributions. The first model is an extension of an older analytical quasi 3D model [14] which was, in its two-dimensional (2D) version, the base of the fitting procedure for the experimental determination of I_r and I_{nr}, as described below. For the simulation of the bulk recombination, we used the 2D drift–diffusion simulator WIAS–TeSCA [15].

In section 2, both models and the fitting procedure are briefly described. In section 3, simulations of the *I–V* characteristics of InGaAs/AlGaAs RW laser diodes are presented and compared with experimental results. A brief summary completes the paper.

2. Modelling

2.1. Surface currents

In order to calculate the current component due to surface recombination, the distribution of the current densities must be known. We consider only the hole current density in the p-doped region because of the broad-area n-contact at the n-doped substrate and the much higher mobility of the electrons. Furthermore, minority currents are neglected. A scheme of the laser diode and its internal current distribution is given in figure 1. The current is injected only along the narrow p-contact stripe. Due to the current spreading effect, a part of the current flows parallel to the junction in the p-doped layer. The only way that this current can leave this layer is by passing through the junction or by non-radiative recombination with electrons at the surface. In figure 1, this current flow is depicted schematically. The model was presented several years ago [16, 17] and will shortly be described in what follows.

The 2D current density $\mathbf{j}_p$ in the p-doped layer contains only a drift component which is proportional to the gradient of the electrostatic potential,

$$\mathbf{j}_p = -\sigma\nabla\varphi, \tag{1}$$

where σ is the hole conductivity and $\nabla = (\partial/\partial x, \partial/\partial y)$. The electrostatic potential φ is measured on the p-side of the junction with respect to the n-type base. On the other hand, an averaging of the continuity equation yields for the current density through the junction

$$j_j = -t\nabla\mathbf{j}_p, \tag{2}$$

where t is the thickness of the p layer. Below laser threshold the current through the p–n junction can be approximated through the well-known expression

$$j_j(x, y) = J_s\, e^{\beta\varphi(x,y)}, \tag{3}$$

where $\exp(\beta\varphi) \gg 1$ has been assumed, J_s denotes the saturation current density and $\beta = q/nkT$ (q elementary charge, n ideality factor and kT thermal energy). The series resistance in the z-direction can be neglected.

Combining equations (1)–(3), we obtain for the potential distribution $\Phi = \beta\varphi$ the partial differential equation

$$\frac{\partial^2\Phi}{\partial x^2} + \frac{\partial^2\Phi}{\partial y^2} - \frac{\beta J_s}{t\sigma}\, e^{\Phi} = 0. \tag{4}$$

Equations (3) and (4) have reduced the originally 3D problem to a 2D one in the x–y plane for $\Phi(x, y)$. Surface recombination currents can be introduced in this plane via the boundary conditions

$$\left.\frac{\partial\Phi}{\partial x}\right|_{x=b/2} = -A\, e^{\Phi(b/2,y)/2} \qquad \text{with} \qquad A = \frac{\beta}{\sigma d} q n_i S_1 L_S \tag{5}$$

$$\left.\frac{\partial\Phi}{\partial y}\right|_{y=L/2} = -B\, e^{\Phi(x,L/2)/2} \qquad \text{with} \qquad B = \frac{\beta}{\sigma d} q n_i S_2 L_S \tag{6}$$

using an ideality factor $n = 2$ as a rough approximation for surface currents according to [18]. S_2 represents the recombination velocity at the front and rear facets, and S_1 the same for the lateral surfaces. L_S is a surface diffusion length [18]. The other boundary conditions are

$$\left.\frac{\partial\Phi}{\partial y}\right|_{y=0} = 0 \qquad \text{and} \qquad \left.\frac{\partial\Phi}{\partial x}\right|_{x=0} = -\frac{\beta}{\sigma} j_0(y) \tag{7}$$

with $j_0(y) = j_{px}(0, y)$ the x-component of $\mathbf{j}_p$ at $x = 0$.

For the whole boundary problem, we have found an analytical solution for $\Phi(x, y)$ as published in [14] and used here for calculations of the *I–V* characteristics including surface currents. Details are given in appendix A. For comparison with experiments, our interest is focused on the calculation of the total current I through the laser diode structure,

$$I = I_e + 2I_0, \tag{8}$$

consisting of the uniform current under the contact stripe I_e and the current I_0 flowing in the region adjacent to the stripe as illustrated in figure 1. The lateral current is given by

$$I_0 = 2t \int_0^{L/2} j_0(y)\,\mathrm{d}y, \tag{9}$$

and the current under the stripe

$$I_e = 2wJ_s \int_0^{L/2} \mathrm{e}^{\Phi(0,y)}\,\mathrm{d}y + 2wqn_i S_2 L_S\,\mathrm{e}^{\Phi(0,L/2)/2} \equiv I_{eb} + I_{es}, \tag{10}$$

where the subscripts b and s refer to bulk and surface components, respectively. Here we have to consider that both contributions to I, I_0 as well as I_e, contain surface currents from outside the stripe or from the facets in the stripe region itself, respectively.

Finally, the forward voltage V is given by $V = \Phi(0,0)/\beta$.

2.2. Extraction of radiative current component and fitting procedure

For our experimental observations of surface currents, the crucial point is to determine the radiative component I_r in the current–voltage (I–V) characteristic and to subtract I_r from the measured current I which provides the non-radiative component $I_{nr} = I - I_r$. This current I_{nr} is the focus of our interest for investigations of surface recombination. The extraction of I_r from the I–V characteristic can be done by a so-called P–V–I analysis, based on an analysis of the power–voltage (P–V) characteristic together with the P–I and I–V dependencies, as we have described it in [10].

The procedure uses the experimental observation that under all surface treatments in our experiments the P–V characteristic remained unaffected, even in cases where the I–V and P–I characteristics showed strong changes.

As outlined in appendix B, for low injection (small voltage) the optical power P is proportional to the current I_j. Therefore, a semi logarithmic plot of the P–V characteristic has to exhibit a straight line in this region of low injection. The appearance of such a straight line in the log(P)–V characteristic is the first criterion for a possible application of the P–V–I analysis. The next one is success in performing an iterative fitting procedure between simulated and measured P–V, P–I and I–V characteristics for the whole current range. This procedure is described in [10–12]. Modelling of P is based on the analytical solution of the current spreading problem, as outlined in the preceding subsection and in appendix A, and explained in appendix B. The analytical model used in the fitting procedure allows a much quicker analysis of experimental P–V–I curves than a numerical solution.

The P–V–I analysis will be illustrated for the case of the I_r determination, as shown in figure 2 and used in figure 4. It starts with a comparison between simulated and measured P–V characteristics. The simulation is performed neglecting surface recombination and non-radiative recombination in the bulk ('infinite' τ_{nr}) which corresponds to an efficiency $\eta_i = 1$ and an identity $I = I_r$ in the low current range according to (B.2) and (B.4). In the experimental $P(V)$ curve the case of low injection is realized, where the straight part of the log(P)–V characteristic appears. Under these conditions, shifting the experimental curve along the logarithmic scaled P axis in figure 2(a), at the coincidence of both curves in the low injection range, the P–V characteristic is identified with the radiative component I_r–V in a first approximation. Such movement of the experimental curve is necessary, because the measured P values are given in relative units and deviate from the simulated ones by an unknown factor. After the determination of I_r–V, it is introduced into the experimental I–V characteristic in figure 2(b), where the difference between I and I_r gives the non-radiative current $I_{nr} = I - I_r$. Using this I_{nr} in figure 2(c) the experimental $P(I)$ curve can be corrected into P–I_r by subtracting I_{nr} in the abscissa from the measured I values. In the double-logarithmic log(P)–log(I) plot, this procedure must lead to a straight line fit along the diagonal of the figure in the low current range (P is expressed in elementary charge times number of photons per second). The calculations of $P(V)$, $I_r(V)$ and $P(I_r)$ are repeated, with the saturation current J_s from equation (3) as a fitting parameter, until correspondence of both the complete P–V and the P–$(I - I_{nr})$ plots in the low injection range are achieved. The I_r–V curve calculated with the final J_s represents the radiative current–voltage I_r–V characteristic for the whole current range, as it is used here in figure 4.

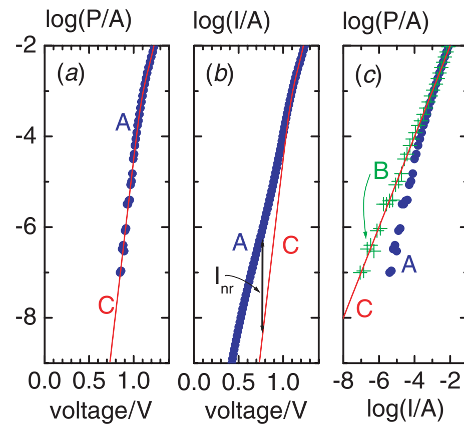

Figure 2. Illustration of P–V–I analysis. P–V (a), I–V (b) and P–I (c) characteristics. Points (A): measured data; full curves (C): extracted radiative current I_r. In (c), pluses (B) denote the measured data (A) corrected by the non-radiative current $I_{nr} = I - I_r$. The optical power P is expressed in elementary charge times number of photons per second.

2.3. Bulk recombination currents

The simulation of the I–V characteristics without accounting for surface recombination was performed with the numerical simulator WIAS–TeSCA [15]. It solves the Poisson equation and the continuity equations for the electron and hole current densities two-dimensionally, taking into account Fermi statistics. At the heterojunctions, continuity of the electron and hole electrochemical potentials is assumed. We simulated the current flow in the plane perpendicular to the junctions and resonator axis (x–z plane). Along the y-axis, the current flow is homogeneous here because of the neglect of the surface recombination. For symmetry reasons, only one-half of the device is simulated.

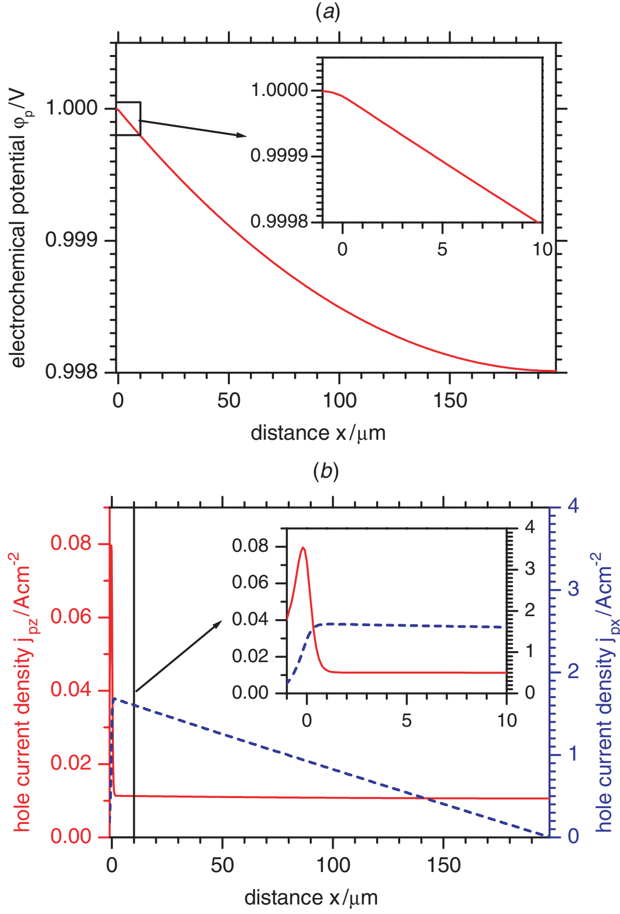

Figure 3. Electrochemical potential (*a*) and hole current densities (*b*) at $V = 1$ V in the p-doped layer above the active zone versus lateral position x. Simulated with WIAS–TeSCA two-dimensionally (no surface recombination). Inset: magnified graphs for $x \leqslant 10\ \mu$m. Full curve in (*b*): z-component (left axis); dashed: x-component (right axis) of hole current density.

The recombination rate entering the continuity equations is given by

$$R = \left[\frac{1}{\tau_n(p + n_i) + \tau_p(n + n_i)} + B_0 + C_n n + C_p p\right](np - n_0 p_0), \quad (11)$$

where n and p are the electron and hole densities, respectively, n_0 and p_0 are the corresponding equilibrium carrier densities and n_i is the intrinsic carrier density. The different term in the brackets describe recombination via deep centres (Shockley–Read–Hall (SRH) recombination), radiative recombination and Auger recombination. In what follows we vary the SRH carrier lifetimes τ_n and τ_p and the coefficient B_0 in order to achieve a correspondence between the simulated and measured I–V characteristics. The Auger coefficients were fixed to $C_n = C_p = 2 \times 10^{-30}$ cm^6 s^{-1}.

In figure 3, the profiles of the electrochemical potential (*a*) and the x and z components of the hole current density (*b*) slightly above the active zone are depicted for a forward bias of 1 V. The carrier lifetimes and radiative recombination coefficient were $\tau_n = \tau_p = 500$ ns and $B_0 = 1.3 \times 10^{-10}$ cm^3 s^{-1}, respectively. It is clearly seen that the current spreads till the device boundary.

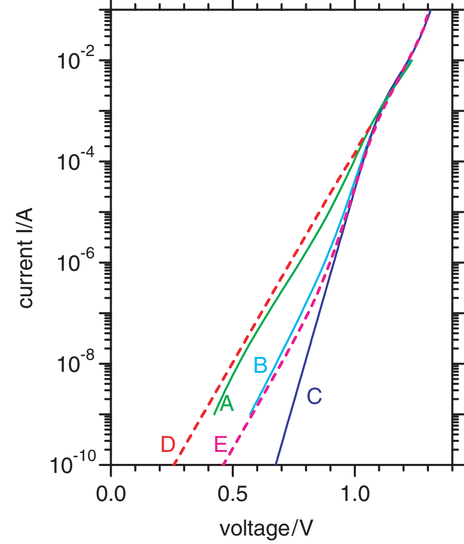

Figure 4. Full curves: experimental current–voltage characteristics before (A) and after $(NH_4)_2S_x$ treatment (B) together with extracted radiative current I_r (C). Dashed: current–voltage characteristics simulated three-dimensionally with surface recombination velocities $S_1 = S_2 = 5 \times 10^6$ cm s^{-1} (D) and 1×10^5 cm s^{-1} (E).

3. Results

3.1. Surface currents in InGaAs/AlGaAs laser diodes

In earlier experiments as cited above [10], we have demonstrated by NH_4S_x surface treatments that below the threshold the non-radiative current component I_{nr} in InGaAs/AlGaAs laser diodes is dominated by surface recombination. Here we relate the observed large reduction of the current over more than one order of magnitude to a corresponding lowering of the surface recombination velocity, S. This is done by the simulation of the current distribution within the diode laser structure, taking into account the surface currents as described in section 2.1.

The experiments were carried out on GaAs-based RW laser diodes emitting at 984 nm. The active zone consisted of two 5 nm thick $In_{0.24}Ga_{0.76}As$ quantum wells (QWs) separated by a 10 nm thick GaAs barrier. It was embedded in GaAs spacer, $Al_{0.28}Ga_{0.72}As$ waveguide and $Al_{0.30}Ga_{0.70}As$ cladding layers. The width of the ridge was 3 μm.

In figure 4, the results of both the simulation and the experiments are shown. Curve A represents the original measured I–V characteristic, curve B the same after the NH_4S_x treatment, and curve C the radiative current component, derived from the 'P–V–I analysis' of the curves A and B as described in section 2.2. Curves D and E are calculated characteristics with $S = 5 \times 10^6$ cm s^{-1} and 1×10^5 cm s^{-1}, respectively.

In the simulations, a constant recombination velocity $S = S_1 = S_2$ was assumed to exist at the (110) and (−110) surfaces. Furthermore, because in our model the surface recombination

is introduced via equations (5) and (6) by the product $n_i \times (S \times L_S)$, we had to estimate values for the intrinsic concentration n_i of the material in which the surface space charge region is localized along the p–n junction perimeter, and the 'intrinsic surface diffusion length' L_S for this region, as defined in [18] for bulk lasers. In multi-layered structures with QWs, as used here in our laser diodes, the n_i and L_S values are given by the materials and by the layer thicknesses around the p–n junction, respectively. In [18], it was already mentioned, that in cases of low layer thicknesses, L_S corresponded to these thicknesses, rather than to the larger diffusion length.

According to scanning electron microscope (SEM) and electron beam induced current (EBIC) measurements, the p–n junction was positioned slightly above the active zone—a more precise localization (with exact correspondence to a layer or interface) was not possible in the frame of the measurement accuracy. From that we estimated the product $n_i \times L_S$ via the intrinsic concentration $n_i = 1.7 \times 10^6$ cm^{-3} of GaAs and $L_S = 2 \times 10^{-6}$ cm as twice the layer thickness of $\sim 10^{-6}$ cm, to be about $n_i \times L_S = 3.4$ cm^{-2}. This value is not so far from the product 2.8 cm^{-2} as it was used in [18] and which is hence applied here, too.

Curves D and E in figure 4 were simulated for a temperature of 300 K with the following parameters: cavity length $L = 1100$ μm, chip width $b = 400$ μm, effective ridge width $w = 5$ μm, active zone (DQW) thickness $t_{AZ} = 1.2 \times 10^{-6}$ cm, conductivity times thickness of the p-type layers $\sigma t = 1.0 \times 10^{-3}$ A V^{-1}, and saturation current density $J_s = 5.6 \times 10^{-24}$ A for the radiative current component, I_r, as final fit from the 'P–V–I analysis'.

Comparing the experimental and simulated characteristics in figure 4, and regarding the original non-radiative current component as being due to surface recombination, we can conclude that the original surface recombination velocity was about 5×10^6 cm s^{-1}. An exact fit is not possible because of the assumed ideality factor $n = 2$ for surface currents and the nonlinear behaviour of the experimental curve (A), obviously due to surface term recharging during the I–V measurement [10]. After the NH_4S_x treatment, the recombination velocity was reduced by a factor of 50 down to about 1×10^5 cm s^{-1}, if we assume that the surface recombination (albeit reduced) is still responsible for the remaining non-radiative current.

3.2. Bulk recombination currents in InGaAs/AlGaAs laser diodes

The remaining non-radiative current component could be also caused by bulk recombination. In this case, the resulting surface recombination velocity is even smaller than 1×10^5 cm s^{-1} as determined above. In order to investigate this, we simulated the I–V characteristics by the numerical simulator 'WIAS–TeSCA' [15] as described in section 2.3, neglecting surface recombination in contradiction to the foregoing interpretation.

In figure 5, the I–V characteristics measured before (curve A) and after (curve B) the NH_4S_x treatment together with the characteristic of the radiative current component C are again shown, identical to figure 4. At first and as a proof, it was necessary to fit the I_r–V characteristic (C). This was done successfully with a simulation using $\tau_n = \tau_p = 10^6$ s

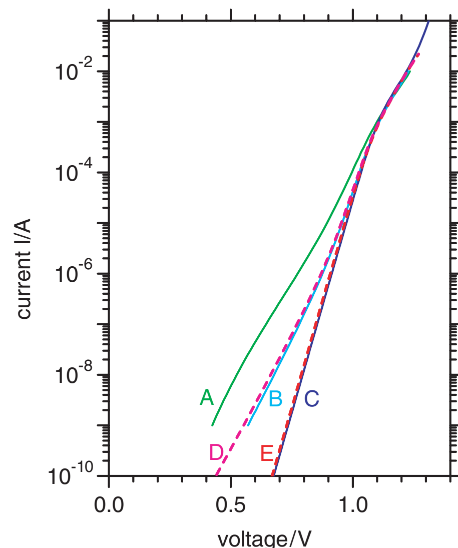

Figure 5. Full curves: experimental current–voltage characteristics before (A) and after $(NH_4)_2S_x$ treatment (B) together with extracted radiative current I_r (C). Dashed: current–voltage characteristics simulated with WIAS–TeSCA two-dimensionally with SRH lifetimes $\tau_n = \tau_p = 500$ ns (D) and $\tau_n = \tau_p = 10^6$ s (E).

('infinite' SRH lifetime) and $B_0 = 1.3 \times 10^{-10}$ cm^3 s^{-1} in the whole structure, giving curve E. The coincidence between curves C and E is remarkable. It demonstrates both the correct extraction of the I_r–V characteristic from the experimental data using the 'P–V–I analysis' and the correct modelling by the numerical simulations with the chosen parameters.

The experimental determination of the radiative current component I_r via the 'P–V–I analysis' is independent of the value of radiative recombination, which was introduced with the coefficient B_0 into the fitting simulation, because of the choice $\eta_i = 1$ in the iterative fitting procedure. Therefore, fitting of the experimentally found I_r–V characteristic with simulations, using infinite carrier lifetimes for the SRH recombination in the bulk, provides the possibility of determination of B_0 itself.

Finally, our interest was focused on a fit of the experimental curve B after the NH_4S_x treatment. Curve D in figure 5 demonstrates, that this was possible with $\tau_n = \tau_p = 500$ ns in the whole laser structure, i.e., inside and outside the QW. Additional calculations have shown that the fitting is almost independent of the lifetimes τ_n and τ_p outside the QW, except for values less than 10 ns. This result means that the non-radiative current which remained after the NH_4S_x treatment could be explained by bulk recombination only. The large values of the SRH lifetimes reveal the high quality of the epitaxial layers in the investigated laser structures. Because in reality the surface recombination did not vanish completely after the NH_4S_x treatment, the bulk SRH lifetimes have to be even higher.

4. Summary

We presented novel investigations of surface and bulk contributions to the non-radiative recombination in InGaAs/AlGaAs ($\lambda = 0.98$ μm) RW laser diodes. These enabled us to explain earlier experiments, in which

we extracted the non-radiative and the radiative current components from the power–voltage–current (P–V–I) characteristics measured well below the threshold. By a comparison of the experimental results with simulations we found a reduction of the surface recombination velocity by a factor of 50 from about 5×10^6 cm s^{-1} down to 1×10^5 cm s^{-1} by a treatment of the facets with NH_4S_x. The non-radiative current component remaining after that treatment can also be explained by non-radiative bulk recombination only with carrier lifetimes greater than 500 ns—a surprisingly high value. We believe, that the presented procedure can be used to qualify special treatments of the facets of laser diodes in order to increase the COMD level and to optimize the epitaxial structure.

Appendix A

Solution of equation (4)

The boundary value problem (4)–(7) of section 2.1 has the analytical solution

$$\Phi(x, y) = c_0 - 2 \ln \psi(x, y) \tag{A.1}$$

with

$$\psi = \left[\frac{\sin(c_1 x + c_2)}{\cos\left(\frac{c_1 b}{2} + c_2\right)} + \frac{B}{A} \frac{\mathrm{ch}(c_1 y)}{\mathrm{sh}\left(\frac{c_1 L}{2}\right)} \right] = \left[\frac{\sin(c_1 x + c_2)}{\alpha_3} + \frac{B}{A} \frac{\mathrm{ch}(c_1 y)}{\gamma_3} \right] \tag{A.2a}$$

or

$$\psi = \left[\frac{\mathrm{ch}(c_1 x + c_2)}{\mathrm{sh}\left(\frac{c_1 b}{2} + c_2\right)} - \frac{B}{A} \frac{\cos(c_1 y)}{\sin\left(\frac{c_1 L}{2}\right)} \right] = \left[\frac{\mathrm{ch}(c_1 x + c_2)}{\eta_3} - \frac{B}{A} \frac{\cos(c_1 y)}{\varepsilon_1} \right] \tag{A.2b}$$

or

$$\psi = \left[\frac{\mathrm{sh}(c_1 x + c_2)}{\mathrm{ch}\left(\frac{c_1 b}{2} + c_2\right)} - \frac{B}{A} \frac{\cos(c_1 y)}{\sin\left(\frac{c_1 L}{2}\right)} \right] = \left[\frac{\mathrm{sh}(c_1 x + c_2)}{\eta_1} - \frac{B}{A} \frac{\cos(c_1 y)}{\varepsilon_1} \right] \tag{A.2c}$$

as we have shown partially (A.2a) in an earlier publication [14]. Here, applying this solution (A.2) for surface current calculations, we have to take into account, that expression (A.1) for the potential together with (A.2a), (A.2b) or (A.2c) is valid for the three regions

$$2\frac{J_s \beta}{\sigma t} > A^2 - \left(\frac{B}{\gamma_3}\right)^2 > 0 \tag{A.3a}$$

and

$$2\frac{J_s \beta}{\sigma t} > B^2 - \left(\frac{A}{\eta_3}\right)^2 > 0 \tag{A.3b}$$

and

$$2\frac{J_s \beta}{\sigma t} > B^2 + \left(\frac{A}{\eta_1}\right)^2 \tag{A.3c}$$

respectively.

Conditions (A.3a) to (A.3c) follow from insertion of expressions (A.1) and (A.2a) to (A.2c) into the differential equation (4) of section 2.1, with the definitions

$$\alpha_3 = \cos\left(\frac{c_1 b}{2} + c_2\right) \tag{A.4}$$

$$\gamma_3 = \mathrm{sh}\left(\frac{c_1 L}{2}\right) \tag{A.5}$$

$$\eta_1 = \mathrm{ch}\left(\frac{c_1 b}{2} + c_2\right), \qquad \eta_3 = \mathrm{sh}\left(\frac{c_1 b}{2} + c_2\right) \tag{A.6}$$

$$\varepsilon_1 = \sin\left(\frac{c_1 L}{2}\right), \qquad \varepsilon_3 = \cos\left(\frac{c_1 L}{2}\right). \tag{A.7}$$

Finally, the I–V characteristic is followed by a point-wise calculation of $[I(c_0), V(c_0)]$ pairs with chosen values of the parameter c_0. The other parameters c_1 and c_2, necessary for the calculation of Φ, are given with c_0 via equation (4) and the boundary conditions (5)–(7) in section 2.1.

Appendix B

Relation between current and emission power

Below the threshold and neglecting surface recombination, the radiative current j_r as a function of the injected δp is given by

$$j_r = q d_{AZ} B_0 (n_0 + \delta p)\delta p. \tag{B.1}$$

Here d_{AZ} denotes the thickness of the active zone (AZ), n_0 the equilibrium majority carrier density (AZ assumed to be of n-type) and B_0 the coefficient of radiative recombination, which is assumed to be constant (actually only valid for Boltzmann statistics).

Due to non-radiative recombination in the bulk, the total current through the junction includes a non-radiative part, too,

$$j_j = j_r + q d_{AZ} \frac{\delta p}{\tau_{nr}} \tag{B.2}$$

where τ_{nr} is the minority carrier lifetime of non-radiative recombination.

For the electroluminescence power P_{VAZ}, per volume of active zone, the dependence of δp can be described with the following expression:

$$P_{VAZ} = q B_0 (n_0 + \delta p)\delta p. \tag{B.3}$$

Equations (B.1) to (B.3) are valid as long as δp exceeds the intrinsic carrier density significantly ($\delta p \gg n_i$). In the absence of surface recombination, both equations (B.1) and (B.3) become independent of the position y and the originally quasi 3D boundary value problems (4) to (7) reduce to a 2D one in the x–z plane, with an x-dependent concentration $\delta p(x)$.

From (B.1) and (B.2) the concentration δp can be derived as a function of the total current $j_j = j$, whereas j itself follows from equations (8) to (10) with solutions (A.1) and (A.2), as described in section 2.1 and appendix A. Insertion of δp from these calculations into (B.3) provides $P_{VAZ}(j)$ and, after integration over the position x, the total emission power in dependence of the total current and the device voltage. This yields finally the P–V–I characteristics without surface recombination.

However at low injection, below the onset of current crowding under the ridge, the current densities j_r and j_j can be assumed as nearly homogeneous over the whole chip area. Hence, the optical power P can be assumed simply proportional to j_j,

$$P_{VAZ} = \eta_i j_j \tag{B.4}$$

with an 'internal' efficiency

$$\eta_i = \frac{B_0(n_0 + \delta p)}{B_0(n_0 + \delta p) + 1/\tau_{nr}}. \tag{B.5}$$

In the 'P–V–I analysis' for j_r determination, as described in section 2.2, the simulations implement 'infinite' lifetimes τ_{nr} or $1/\tau_{nr} = 0$, which leads to an identity between the densities P_{VAZ} and $j_r = j_j$ or the total values P and I, at low injection. This will be used in the corresponding fitting procedure between the simulated and measured $P(V)$ curves, when in the low current region, where proportionality (B.4) is satisfied, the measured $P(V)$ characteristic is identified with the simulated $I_r(V) = I(V)$ curve.

References

[1] Hayashi I 1980 Degradation in III–V opto-electronic devices *J. Phys. Soc. Japan* **49** (Suppl. A) 57–65

[2] Ueda O 1996 *Reliability and Degradation of III–V Optical Devices* (Boston, MA: Artech House Publishers)

[3] Eliseev P G 1991 *Reliability Problems of Semiconductor Lasers* (New York: Nova Science Publishers)

[4] Fukuda M 1991 *Reliability and Degradation of Semiconductor Lasers and LEDs* (Boston, MA: Artech House Publishers)

[5] Chen G and Tien C L 1993 Facet heating of quantum well lasers *J. Appl. Phys.* **74** 2167–74

[6] Tang W C, Rosen H J, Vettinger P and Webb D J 1991 Evidence for current-density-induced heating of AlGaAs single-quantum-well laser facets *Appl. Phys. Lett.* **59** 1005–7

[7] Jakubowicz A 1997 Material and fabrication-related limitations to high-power operation of GaAs/AlGaAs and InGaAs/AlGaAs laser diodes *Mater. Sci. Eng.* B **44** 359–63

[8] Chand N, Hobson W S, de Jong J F, Parayanthal P and Chakrabarti U K 1996 ZnSe for mirror passivation of high power GaAs based lasers *Electron. Lett.* **32** 1595–6

[9] Hashimoto J-I, Ikoma N, Murata M and Katsuyama T 1998 Highly reliable GaInAs/GaInP 0.98 μm window laser *Proc. 16th ISCL (Nara, Japan, Oct. 1998)* pp 131–2

[10] Beister G, Maege J, Erbert G and Tränkle G 1998 Non-radiative current in InGaAs/AlGaAs laser diodes as a measure of facet stability *Solid-State Electron.* **42** 1939–45

[11] Beister G, Maege J, Gutsche D, Erbert G, Sebastian J, Vogel K, Weyers M, Würfl J and Daga O P 1996 Simple method for examining sulphur passivation of facets in InGaAs–AlGaAs ($\lambda = 0.98$ μm) laser diodes *Appl. Phys. Lett.* **68** 2467–8

[12] Beister G, Maege J, Sebastian J, Erbert G, Weixelbaum L, Weyers M, Würfl J and Daga O P 1996 Stability of sulphur-passivated facets of InGaAs–AlGaAs laser diodes *IEEE Photonics Technol. Lett.* **8** 1124–6

[13] Sandroff C-J, Nottenburg R N, Bischoff J-C and Bhat R 1987 Dramatic enhancement in the gain of a GaAs/AlGaAs heterostructure bipolar transistor by surface chemical passivation *Appl. Phys. Lett.* **51** 33–5

[14] Beister G, Maege J and Richter G 1988 Identification of surface influences on the current–voltage characteristics of narrow oxide stripe laser diodes *Phys. Status Solidi.* a **105** K45–9

[15] Gajewski H *et al* 2000 *WIAS–TeSCA—Two- and Three-Dimensional Semiconductor Analysis Package* (Berlin: Weierstrass Institute for Applied Analysis and Stochastics)

[16] Joyce W B and Wempel S H 1970 Steady-state junction-current distributions in thin resistive films on semiconductor junctions *J. Appl. Phys.* **41** 3818–30

[17] Yonezu H, Sakuma I, Kobayashi K, Kamejima T, Ueno M and Nannichi Y 1973 A GaAs–AlGaAs double heterostructure planar stripe laser *Japan. J. Appl. Phys.* **12** 1585–92

[18] Henry C H, Logan R A and Merritt F R 1978 The effect of surface recombination on current in $Al_xGa_{1-x}As$ heterojunctions *J. Appl. Phys.* **49** 3530–42